Contents lists available at ScienceDirect

Energy Storage Materials
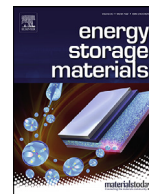
Development of Magnesium Borate Electrolytes: Explaining the Success of Mg[B(*hfip*)$_4$]$_2$ Salt

Piotr Jankowski [a,b,*], Zhenyou Li [c], Zhirong Zhao-Karger [c], Thomas Diemant [c], Maximilian Fichtner [c,d], Tejs Vegge [a], Juan Maria Garcia Lastra [a]

[a] *Department of Energy Conversion and Storage, Technical University of Denmark, Kgs. Lyngby, 2800 Denmark*
[b] *Faculty of Chemistry, Warsaw University of Technology, Warsaw, 00-661 Poland*
[c] *Helmholtz Institute Ulm (HIU) Electrochemical Energy Storage, Helmholtzstraße 11, Ulm, D-89081 Germany*
[d] *Institute of Nanotechnology, Karlsruhe Institute of Technology (KIT), Hermann-von-Helmholtz-Platz 1, Eggenstein-Leopoldshafen, D-76344 Germany*

ABSTRACT

Magnesium batteries are one of the most promising post-lithium technologies. One of the main challenges preventing its commercialization is to find an efficient and safe electrolyte. The electrolyte, playing the role of the blood in a battery, interacts with all battery components and must be highly compatible with all of them. The development of Cl-free electrolyte systems is desired to avoid corrosion issues, and many studies suggest magnesium tetrakis(hexafluoroisopropyloxy)borate ($Mg[B(hfip)_4]_2$) as one of the best candidates in terms of electrochemical properties and chemical stability. Here we present an in-depth analysis of the unique structure of this salt and the interactions generated in the electrolyte among the dissociated ions. The results show a delicate balance between electron-withdrawing effects and ligand stabilization in $B(hfip)_4^-$, crucial from the point of view of magnesium electrolytes. Moreover, the bulk nature of $B(hfip)_4^-$ limits the anion-cation contacts to infrequent interactions through fluorine atoms. This has consequences not only for ion transport but also for hindering the anion decomposition towards the formation of MgF_2. Taken together, we managed to demystify the exclusive nature of $B(hfip)_4^-$ anion, thereby allowing for further rational development of new anion structures.

1. Introduction

Rechargeable batteries are becoming increasingly necessary in our daily life, and the need for higher energy density storage is pushing the research beyond the currently predominant lithium-ion batteries. [1] Additionally, the expected huge increasing demand for batteries requires considering the availability of raw materials, such as lithium, cobalt, or nickel, and the impact of their mining. Lithium is scarcely found in the Earth's crust and is only accessible in a few countries, thus desired direction is not only to change the cathodes based on nickel and cobalt but also switch battery chemistry to another alkali or even alkaline earth metal. Magnesium batteries are one of the alternative technologies, employing magnesium metal as anode with high theoretical volumetric capacity (3833 mA h cm^{-3}) and a relatively low reduction potential (−2.37 V *vs.* SHE). [2] The divalent character of magnesium cation offers two electrons per atom during electrode reaction, and with a properly designed electrolyte and cathode, one can expect to obtain a practical battery with an energy density of at least 320 Wh kg^{-1}. [3–5] This makes the magnesium technology attractive, but many efforts are needed to enable its commercialization.

Electrolytes that provide reversible magnesium plating/stripping reactions are limited. [6] Many typical organic solvents used in lithium-ion batteries form passivation films on the anode surface, inhibiting the passage of magnesium cations. [7,8] Ethers, especially tetrahydrofuran

and glymes, have been found to be compatible with magnesium metal. However, the choice of salt has been an open question for a long time. [6,9–11] The presence of organometallic species or chlorine anions was shown many times to enable the anode reaction. Still, their hazardous and corrosive nature, together with low anodic stability, discourage application in the commercial product. [12] Thus, the development of Cl-free electrolyte systems has been pursued.

Many different anions have been proposed and studied, showing the possibility of reversible electrode reactions. Aromatic anions, based on cyclopentadiene and imidazolium structures, were proven to enable reversible reactions, although offering low oxidation stability – below 2 V *vs.* Mg. [13–15] Similar results were obtained for $Mg(BH_4)_2$, with a bit higher anodic stability, enabling the cycling of Mg/Chevrel Phase battery. [16] The anodic stability was shown to be significantly improved when the boron-center structure of $Mg(BH_4)_2$ was replaced by a boron-cage structure, namely $Mg(CB_{11}H_{12})_2$. $Mg(CB_{11}H_{12})_2$-based electrolyte was reported to be stable up to 3.5 V *vs.* Mg, providing at the same time reversible Mg deposition/stripping and an efficiency higher than 98%. [17] The excellent performance of $Mg(CB_{11}H_{12})_2$ is unfortunately connected with the unique structure of its anion, which is difficult to synthesize and thus very expensive. Hence, new research efforts focused on modifying the boron-center anions by providing electron-withdrawing ligands. [18] This gave rise to the development of the $Mg[B(hfip)_4]_2$ salt, which was created using hexafluoroisopropanol (hfip) as a ligand.

P. Jankowski, Z. Li, Z. Zhao-Karger et al.

[19] The electrochemical studies with this salt showed high oxidative stability (~4 V *vs.* Mg), high ionic conductivity, and excellent Coulombic efficiency of Mg deposition. These features of Mg[B(*hfip*)$_4$]$_2$ salt made it the most promising one among the current state-of-the-art Cl-free magnesium electrolytes. The most important question that comes into mind when looking at the Mg[B(*hfip*)$_4$]$_2$ salt is the origin of its superior properties. The hexafluoroisopropanol is well known in chemistry as a versatile solvent and ligand, [20] but an in-depth analysis targeting its electrochemical properties were never performed.

Here we are making an effort to explain the outstanding balance of the hfip ligand, first by comparing it to other potential salts created thanks to molecular engineering and then looking at the interactions inside the electrolyte and its eventual reactions at the anode surface. To support all of our findings based on computational insight at the molecular level, the theoretical analysis was combined with experimental studies, thereby proving its correctness.

2. Methodology

2.1. Experimental studies

The magnesium tetrakis(hexafluoroisopropyloxy)borate Mg[B(*hfip*)$_4$]$_2$ was synthesized by refluxing magnesium borohydride Mg(BH$_4$)$_2$ and hexafluoroisopropanol in monoglyme at 85 °C. Mg(BH$_4$)$_2$ in turn was produced in-house from a reaction between sodium borohydride and magnesium chloride. [21] The final solid product was characterized by nuclear magnetic resonance spectroscopy (NMR). The corresponding ^{1}H-, ^{19}F- and ^{11}B-NMR spectra were collected with a Bruker Advance II 500 spectrometer, using tetrahydrofuran d8 as solvent, and presented in Figure S1. To prepare various Mg[B(*hfip*)$_4$]$_2$-based electrolytes, the Mg[B(*hfip*)$_4$]$_2$ powder was dissolved in anhydrous ethereal solvents (tetrahydrofuran – THF, monoglyme – G1, or diglyme – G2) with defined concentrations (0.1 M, 0.3 M and 0.5 M).

Infrared spectra were recorded on a Spectrum Two (PERKIN ELMER) Fourier-transform infrared spectrometer, using a diamond crystal attenuated total reflection (ATR). The spectra were collected in absorbance mode with 4 scans at a resolution of 4 cm^{-1} in the range of 4000 to 400 cm^{-1}. All measurements were conducted inside an argon-filled glovebox.

To study Mg deposits, chronopotentiometry was carried out in Mg-Mg symmetric cells with the Mg[B(*hfip*)$_4$]$_2$-based electrolytes. Borosilicate glass fiber GF/C was applied as a separator. The measurement was performed by plating and stripping at 0.1 mA cm^{-2} for 30 min for 5 cycles, using a Biologic VMP-3 potentiostat. The operating temperature was 25±0.1 °C. The cycled electrodes were soaked in G1 for 3 h and further washed with G1 3 times before vacuum drying overnight.

X-ray photoelectron spectroscopy (XPS) measurements were conducted using a PHI 5800 MultiTechnique ESCA system (Physical Electronic). The spectra were acquired using monochromatic Al K$_\alpha$ (1486.6 eV) radiation, a detection angle of 45°, and a pass energy of 29.35 eV at the analyzer for detailed measurements. XPS measurements were also collected after Ar$^+$ ion sputter treatment of the samples (for 3 and 10 min, sputter rate ~1 nm min^{-1}) to create a depth profile. For binding energy calibration, the C1s peak of adventitious C on the electrode surface was used as a reference and set to 285.0 eV on the unsputtered surfaces. In comparison, after sputtering (and almost complete removal of the adventitious C), the F1s peak of MgF$_2$ was used instead and set to 685.7 eV. With that procedure, the Mg2p peak of metallic Mg stays at 49.5 eV in all measurements. To avoid surface contamination, the samples were transferred in an inert gas atmosphere to the sample load lock of the XPS system.

2.2. Computational studies

The computational study of Mg[B(*hfip*)$_4$]$_2$ salt was carried out using Density Functional Theory (DFT) simulations. We used the Gaussian 16 package [22], employing the M06–2X [23] DFT functional and Pople 6–31++G(d,p) basis set. To mimic the electrolyte surrounding the conductor-like polarizable continuum model (C-PCM) using parameters for THF was applied for all calculations. As a starting point, we performed a screening through different possible ligand structures. 24 different anions were generated, and the search for their optimal geometry was performed by DFT optimization of 20 random conformation geometries created with the conformation search tool implemented in Gabedit software [24]. The geometry with the lowest energy was considered as the ground state of each anion. To search for the most preferred geometry of cation-anion pairs, the three lowest energy anion geometries were considered. The magnesium cation was added in 10 random positions for each of them, generating in total 30 starting geometries for DFT optimization. The structures with the lowest energy after optimization were considered as the ground state of the ion pairs. The interaction energy between anion and cation was calculated as a difference in free energies of separate ions and ion-pair:

$$E_{int} = G_{Mg2+} + G_{anion} - G_{ion-pair}$$

The ground state geometries were also used to assess the electrochemical stability of the salt. Our initial results indicated free anions to be the most sensitive towards oxidation, and ion-pairs the easiest to be reduce, determining overall oxidation and reduction limits (Table S1), in line with many previous studies in the literature. [25–29] Thus, to determine the oxidation limit, the geometry of the anion was reoptimized after removal of a single electron; to determine reduction limit, the geometry of ion-pair was reoptimized after insertion of an extra electron. The electrochemical stability limit potential was calculated as follow and converted to V *vs.* Mg scale by subtracting 2.14 V [30]:

$$E_{ox} = (G_{anionox} - G_{anion})/F - 2.14 \, [\text{V vs. Mg}]$$

$$E_{red} = -(G_{ionpairred} - G_{ionpair})/F - 2.14 \, [\text{V vs. Mg}]$$

The optimized reduced ion pair geometries were further analysed for the stability of B–O, O–C, and C–F bonds. In each of the case, the bond cleavage was forced by extending the bond length by *ca.* 2 Å and reoptimizing the structure under this constrain. After breaking the bond, the change in free energy with respect to the ground state structure was reported and analyzed, indicating thermodynamic force towards the studied decomposition.

A more detailed analysis of the Mg[B(*hfip*)$_4$]$_2$ system was performed by explicitly including solvent molecules of G1, G2, and THF in the simulations while keeping the same computational setup as above. Complexes of separated, fully solvated cation and anion (Mg(O$_{solv}$)$_6$$^{2+}$•B(hfip)$_4$$^-$) were taken as a starting point, and the number of oxygen atoms around magnesium was reduced step by step simulating an increase in salt concentration. Five starting geometries were considered for each of the steps, and the one with the lowest energy was reported. Vibrational spectra were obtained for all optimized geometries, and rescale by a factor 0.95 to adjust to the experimental results, as a standard procedure to compensate the discarded anharmonicity. [31] The reduction ability of the complexes was examined by optimizing the structure after injection of an additional electron and calculating the reduction potential as above. Due to computational limitations, the presence of Mg metal anode during the electron transfer process has been neglected, assuming that all complexes are affected in the same way by the metal anode. The stability of the reduced clusters was tested by the controlled breaking of specific bonds, both in the structure of solvent and anion. For the paths with a negative change in free energy, the kinetic barrier was determined by searching for transition state geometries.
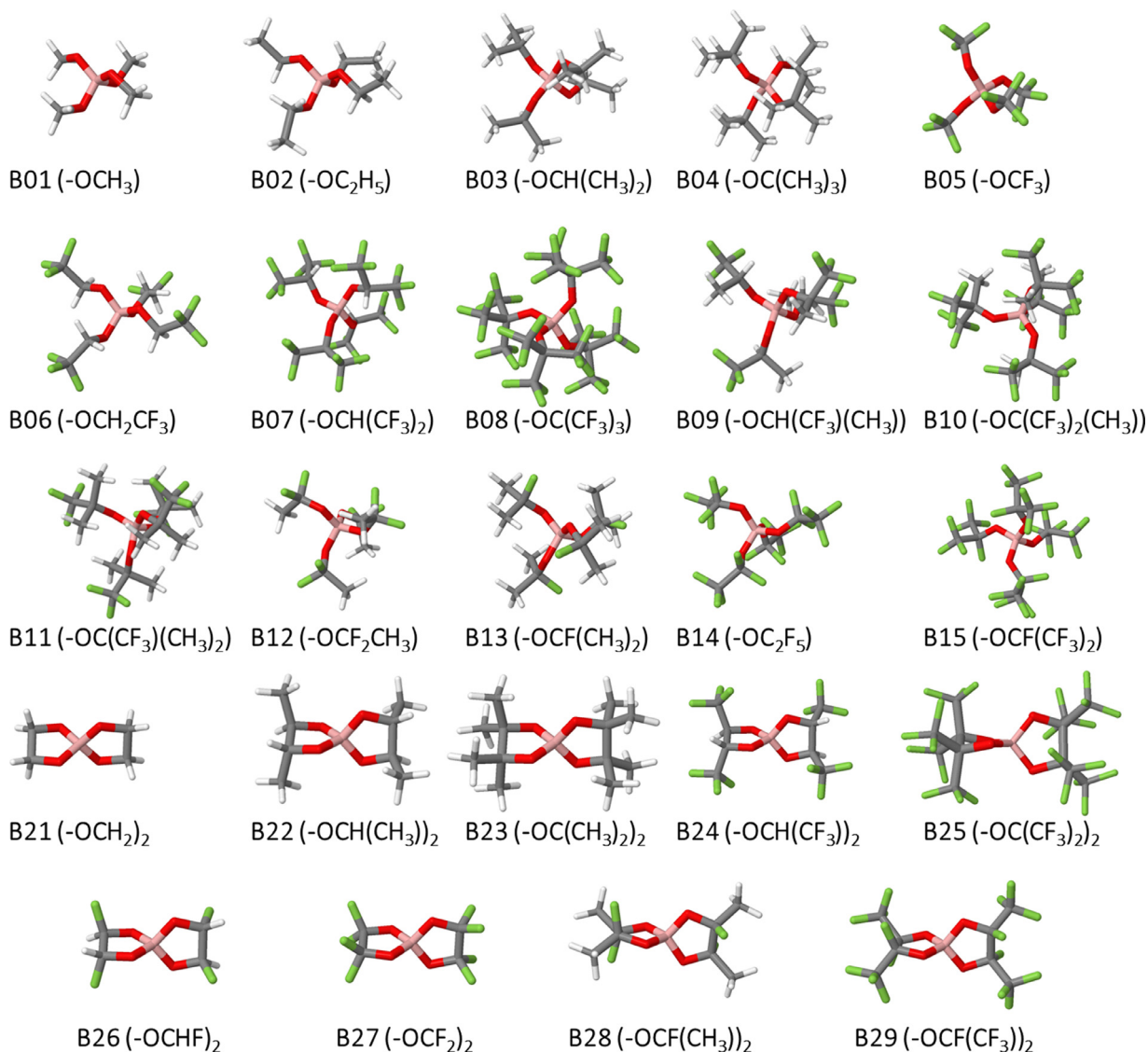
ARTICLE IN PRESS

JID: ENSM [m5GeSdc;November 16, 2021;12:36]

P. Jankowski, Z. Li, Z. Zhao-Karger et al. Energy Storage Materials xxx (xxxx) xxx

Fig. 1. Structures of anions are considered in the screening process. Chemical formulas of the single ligands are indicated next to their labels. Atom colors: B pink, O red, C gray, H white, F green.

3. Results

3.1. Impact of ligand structure on anion properties

To find the connection between the structures of anions with the performance of the magnesium electrolyte, we probed the system with different ligands connected to a boron center atom. More precisely, 15 different monodentate (B01-B15) and 9 bidentate (B21-B29) ligands with different structural features were considered, creating in total 24 different boron-centered anions with different degrees of substitution and fluorination (Fig. 1). For each of the created anions, we tested basic descriptors that can indicate the interaction strength and stability in the electrolyte.

A vast range of values is observed, focusing on the interaction energy between anions and cations (Fig. 2a, right axis). The strongest interactions are predicted for the structures without any fluorine atoms in the structure (B01–04, B21–23). That proves the beneficial role of fluorine substitution in delocalizing the negative charge of the anion and thus in reducing the interaction between ions. The impact of that can be exemplified by looking at the stepwise fluorination of –OCH(CH$_3$)$_2$ ligand

(B03: 336 kJ mol^{-1}):

*B*03 :	$-OCH(CH_3)_2$	336 kJ mol^{-1}
*B*13 :	$-OCF(CH_3)_2$	250 kJ mol^{-1}
*B*09 :	$-OCH(CH_3)(CF_3)$	243 kJ mol^{-1}
*B*07 :	$-OCH(CF_3)_2$	151 kJ mol^{-1}
*B*15 :	$-OCF(CF_3)_2$	74 kJ mol^{-1}

Exchange of the single proton to fluorine (–OCF(CH$_3$)$_2$; B13: 250 kJ mol^{-1}), or perfluorination of one of the methyl groups (–OCH(CF$_3$)(CH$_3$); B09: 243 kJ mol^{-1}) leads to a reduction of interaction by *ca.* 90 kJ mol^{-1}. Going further, perfluorination of the second methyl group decreases energy again by *ca.* 100 kJ mol^{-1} (–OCH(CF3)$_2$; B07: 151 kJ mol^{-1}), and replacement of the last hydrogen atom by fluorine atom reduces the value by an additional 77 kJ mol^{-1}, resulting in a very weak interaction (–OCF(CF$_3$)$_2$; B15: 74 kJ mol^{-1}). Indeed, the anions with the lowest interaction energies are perfluorinated (B08, B15, B25, B29), with the lowest value found for B08 – only 22 kJ mol^{-1}. That indicates the need for fluorine atoms in order to enhance dissociation of the salt. The other structural properties, like, for instance, the size of
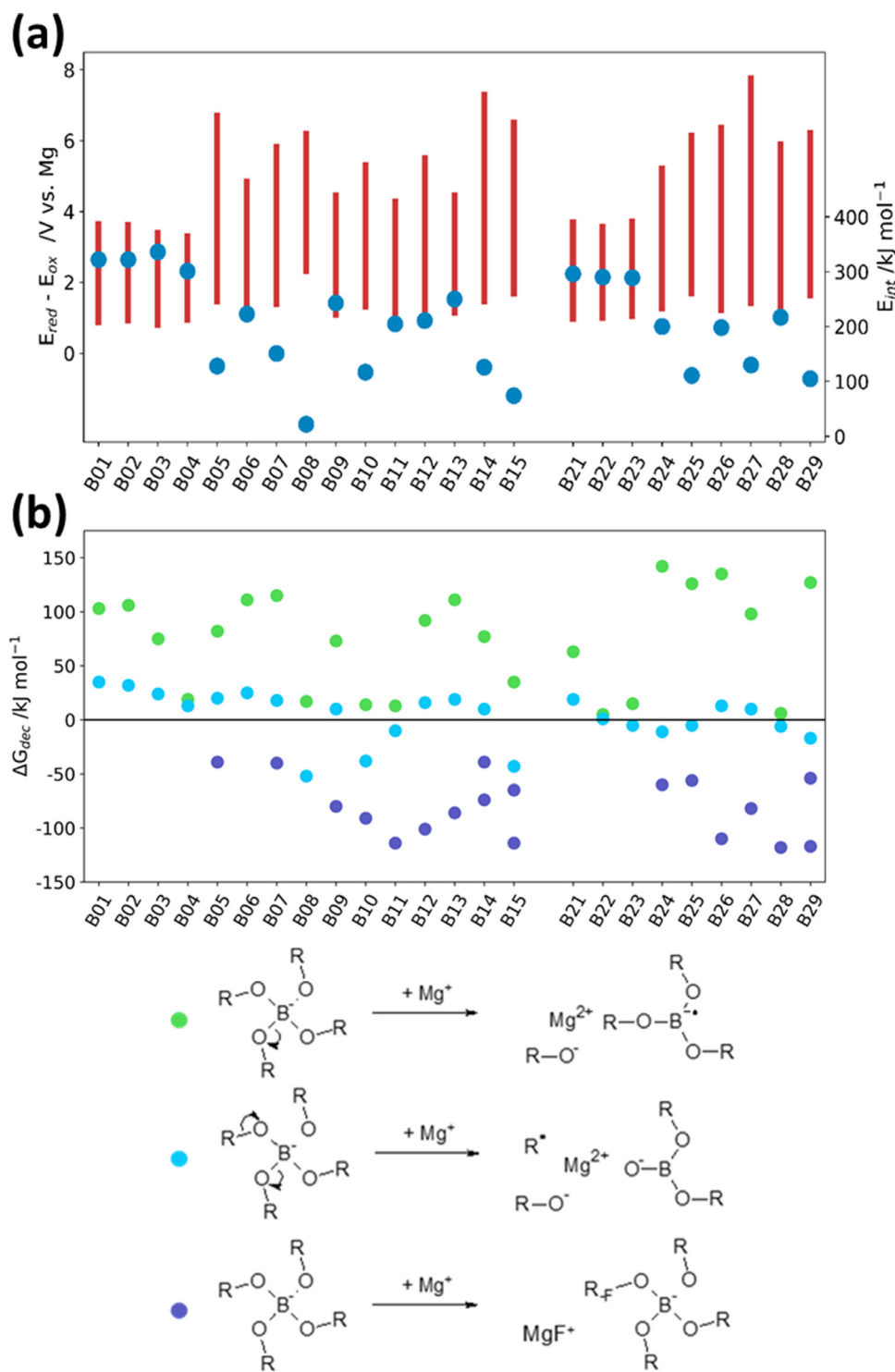
Fig. 2. (a, lefts axis) Electrochemical stability of different salts: E_{red} calculated as addition of an electron to ion pair MgA^+, E_{ox} calculated as removal of an electron from anion A^-; (a right axis) interaction energy between magnesium cation (Mg^{2+}) and single anion (A^-); (b) free energies for different decomposition mechanisms of reduced MgA^0.

the ligand, were found to have a much lower impact on the interaction energy: A comparison of non-fluorinated monodentate (B01-B04) and bidentate ligands (B21-B23) showed only a slow decrease upon increasing the size, with all their interaction energies lying in a narrow span from 290 to 320 kJ mol^{-1}.

Coming to the second descriptor, the electrochemical stability window was determined using the oxidation potential related to the single anion and the reduction potential corresponding to the Mg^{2+}-A^- ion pair, as done in previous works (Fig. 2a left axis). [18] Additionally, HOMO and LUMO were analyzed, giving information regarding oxida-

tion/reduction centers (Figures S2-S3). The charge analysis reveals that there is no distinct part of anion that undergoes oxidation. Conversely, the entire anion is affected by electron removal (Table S2). The enormous impact of the fluorination was also confirmed here: the presence of fluorine atoms increases the oxidation potential (upper limit of the bars at Fig. 2a). The impact of fluorination is highly dependent on the place of substitution: the introduction of fluorine closer to the boron center results in a larger change than –OCF$_2$CH$_3$ (B12: 5.60 V $vs.$ Mg) to –OCH$_2$CF$_3$ (B06: 4.91 V $vs.$ Mg). Thus the highest values are found for small perfluorinated structures, $e.g.$, B05, B15, and B27 (7.8 V $vs.$

ARTICLE IN PRESS

JID: ENSM [m5GeSdc;November 16, 2021;12:36]

P. Jankowski, Z. Li, Z. Zhao-Karger et al. Energy Storage Materials xxx (xxxx) xxx

Mg). Nevertheless, any anion with at least one fluorine atom shows good anodic stability >4.3 V *vs.* Mg, indicating the necessity of partial fluorination both from the point of view of oxidation stability and lowering the ionic interaction. Looking at the other side of the electrochemical stability range (lower limit of the bars at Fig. 2a), we found that the reduction potentials for all tested ion pairs are above 0 V *vs.* Mg, indicating their possible decomposition at the negative electrode. High values are partially connected with the presence of barely solvated magnesium cation, prone to accept electrons. Analysis of charges in the molecules confirms that extra electron is initially predominantly located at magnesium cation. However, if the unoccupied orbitals at the anion are energetically low enough, the partially reduced cation (Mg^+) can transfer electrons and initiate an undesired decomposition of the anion.

To further study this issue, we looked at possible decomposition paths (Fig. 2b), considering the breaking of different bonds in the reduced ion pair $Mg-A^0$ structure: B–O, O–C, and C–F. Negative values of the free energy of the reaction indicate a thermodynamic preference towards the decomposition of the anion. Indeed, we were able to detect such paths for most of the tested anions. Starting with the B–O breaking mechanism (Fig. 2b, green dots), our results indicate that such a path is not energetically favorable for any of the analyzed anions. Positive values indicate the stability of B–O bond, although some of the anions values are very close to 0 kJ mol^{-1}. A different situation was observed when simulating the cleavage of O–C bond (Fig. 2b, blue dots). Due to the huge charge density of the remaining oxygen atom next to boron, the dissociation of another B–O bond was always observed. The decomposition mechanism of the reduced $MgB(OR)_4^0$ towards $BO(OR)_2$, MgOR and R• results in a change in free energy close to 0 kJ mol^{-1}, being exo- or endothermic depending on the specific anion. That seems to be a critical aspect when designing this class of anions, as such a path results into the decomposition of the $MgB(OR)_4$ anion to MgOR, with much higher interaction energy. Looking at the values, two important factors are seen as the driving force to shift the equilibrium towards decomposition products: i) The stabilization of OR$^-$ anion by the presence of strongly withdrawing groups; ii) The stabilization of R• radical by a higher level of substitution. That explains why lower values were observed for anions made of bidentate ligands (B21-B29), as well as much lower values of free energy of reaction for $-OC(CF_3)_3$ (B08: -52 kJ mol^{-1}), $-OCF(CF_3)_2$ (B15: -43 kJ mol^{-1}) and $-OC(CF_3)_2(CH_3)$ (B10: -38 kJ mol^{-1}). Thus, it is crucial is to achieve the right balance between the withdrawing force of the entire ligand, to minimize ion interaction and maximize anodic stability. The level of substitution to prevent radical stabilization and shift toward decomposition products. Therefore, the presence of a proton at the alpha carbon seems to be the optimal way to maintain the right balance. The anions fulfilling these requirements (B01–03, B06–07, B09) are resistant to that decomposition mechanism. Finally, we tested the mechanism involving the dissociation of C–F bonds (Fig. 2b, violet dots). This was only tested for fluorinated anions, finding instability for all of them. The formation of MgF_2 is always thermodynamically preferred. Unfortunately, our studies do not indicate any direction to stabilize C–F bonds thermodynamically. The consequence of potential MgF_2 formation is also unknown. However, recent studies have shown lower magnesium diffusion barriers in MgF_2 relative to other inorganic compounds. [32] Thus the formation of MgF_2 thin layers may still allow for the Mg striping and deposition at the anode.

Concluding our screening procedure, the selection of proper ligand as a building block for magnesium borate salt aims at reaching a delicate balance between low cation-anion interaction energy, high anodic stability, and stability against undesired reductive decomposition. Some correlation between ionic interaction and reduction and oxidation stability can be found, as all of them are largely influenced by charge delocalization (Figure S4). In principle, ligands with high withdrawing force are desired, as they lower the ionic interaction and improve the oxidation stability. However, they are at the same time able to shift the fragile equilibrium of reductive decomposition towards the products. The way to balance that issue is to lower substitution at alpha carbons,

thus making the formed radical less stable. That explains the uniqueness of $B(hfip)_4^-$ anion (B07): (i) The hfip ligand backbone is based on an isopropyl group with two out of the three hydrogen atoms bonded to the central carbon atom are substituted by methyl groups. This configuration provides the system a degree of freedom for distributing the negative charge among the new methyl groups. The fact that one hydrogen is not substituted prevents a radical detachment which most likely would occur if all the hydrogens were replaced by methyl groups (tertiary radicals are more stable than secondary ones); (ii) All beta carbons are fully substituted with fluorine atoms. The latter provide electron-withdrawing force to the ligand promoting delocalization of negative charge thus lowering interaction with cation and hindering the removal of electrons (increasing oxidation stability); concomitantly the newly created highly polarized C–F bonds promotes accepting extra electrons (reduction) and bond dissociation; (iii) The alpha carbon is left non-fluorinated. The central carbon atom is the most sensitive part of the ligand, where a possible radical would be predominately located; the fluorination of the remaining hydrogen at that carbon would introduce a weak spot, promoting defluorination and thus anion decomposition. Thus, the remaining proton is a critical structural factor for the hfip ligand. Taken together, the structure of hfip ligand results in $B(hfip)_4^-$ anion with low interaction energy, high oxidation stability and shifted cathodic stability of the borate core structure. The only remaining reductive decomposition of such anion is defluorination, which is described henceforward.

3.2. Solvation of Mg[B(hfip)$_4$]$_2$ salt in ethereal solvents

The dissolution of the salt in the solvent results in the solvation of magnesium cations, and ideally, in their separation from anions. Approximating the interaction of bare ions with the solvent molecules by using an implicit model is too crude and usually turns out to be unreliable. Thus, an explicit solvent model that includes at least the first coordination shell of the ions is required to obtain meaningful results. Indeed, our recent continuum modeling studies indicated the importance of solvent content on the ion agglomeration in Mg[B(*hfip*)$_4$]$_2$/G1 electrolyte. [33] To get more knowledge regarding the structure of the Mg[B(*hfip*)$_4$]$_2$ electrolytes, we considered its solvation in the three most common ethereal solvents, namely: tetrahydrofuran (THF), monoglyme (G1), and diglyme (G2). In case of G1, crystallographic studies suggest a full separation of anions and cation, thanks to the complete solvation of magnesium cation by G1 at low salt concentrations [19] and thus we assumed the same situation for all three solvents. Such solvent separated ion pairs have been simulated, showing significantly decreased anion-cation interaction energies: from 191 kJ mol^{-1}, for bare cation-anion ion pair, to 82, 74, and 71 kJ mol^{-1}, for anion interaction with full solvation of magnesium cation by THF, G1, and G2 solvent molecules, respectively. Therefore the assumption of having the Mg cations completely solvated only holds if a tremendous excess of solvent over salt is present, especially when considering the solvation of the two bulky $B(hfip)_4^-$ anions per every magnesium cation. Thus, in a more realistic situation, some interaction between magnesium cations and anions may be expected. To determine these changes in the electrolyte, we attempted to simulate with DFT the situation of increasing salt concentration by gradually removing the solvent sites from the coordination sphere of magnesium (Fig. 3). Interestingly, our calculations show an increase in energy upon such this process, confirming a high driving force for the cation solvation of Mg[B(*hfip*)$_4$]$_2$ in ethereal solutions. Subsequent removal of THF molecules makes the magnesium cation to interact with the anion (Fig. 3a): initially through fluorine atom(s), and after the elimination of three THF molecules, the solvation shell becomes small enough to enable a closer approach of the anion closer that creates a direct interaction with the oxygen atom(s) of the anion. This last step significantly affects the thermodynamics of the process: while the initial replacement of O_{THF} to F_{hfip} requires an energy of more than 100 kJ mol^{-1}, the switch from O_{THF} to O_{hfip} is 4 times less energetic or even
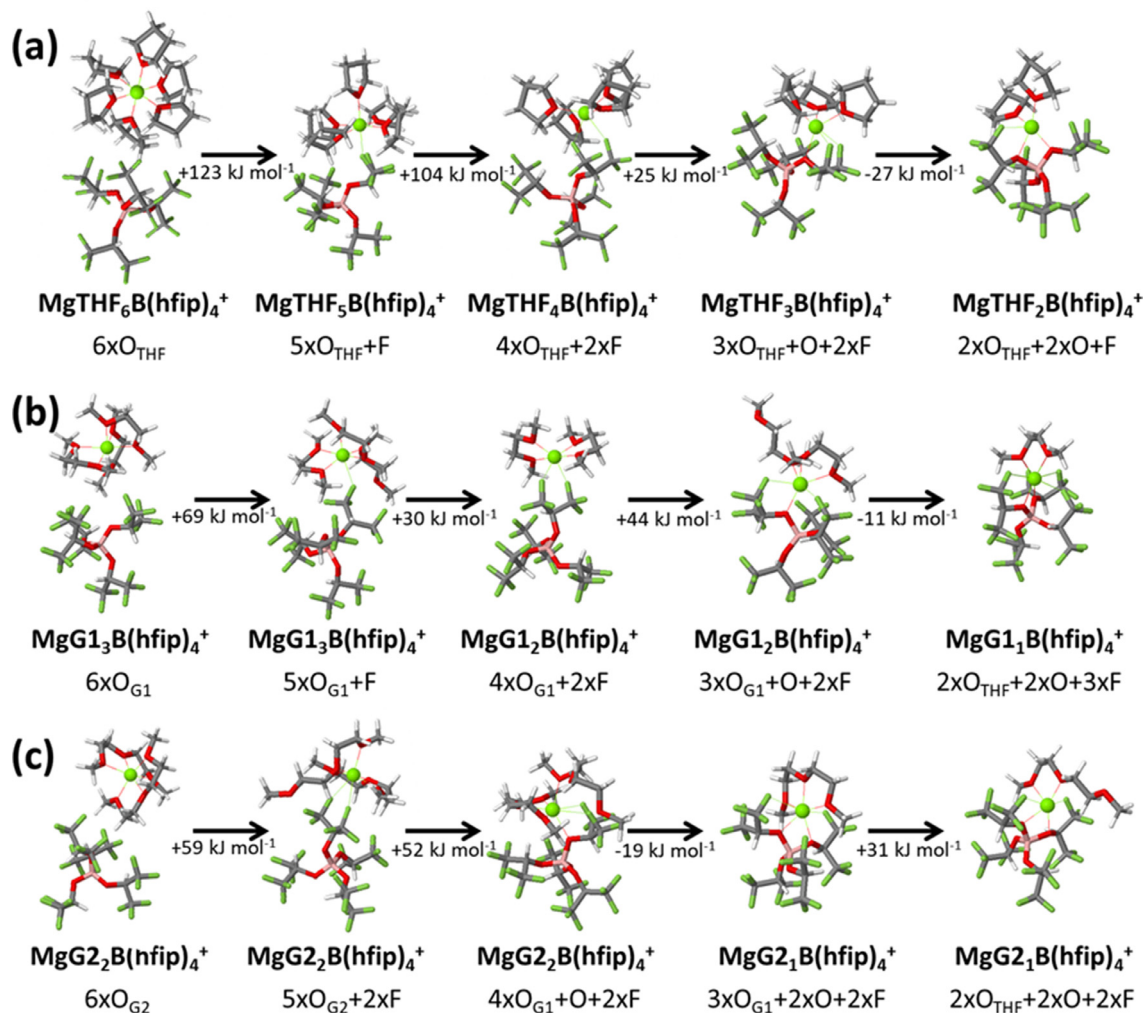
Fig. 3. Aggregation process upon decreasing solvent content of Mg[B($hfip$)$_4$]$_2$ in a) THF, b) G1, and c) G2. The values indicate the change in free energies during the reaction.

favoured when the second O_{hfip} comes into play. A similar situation is observed when G1 is used to solvate magnesium cations (Fig. 3b). However, lower energies are required to initiate the interaction of the anion with the magnesium cation (69 kJ mol^{-1} for G1 in comparison to 123 kJ mol^{-1} in a THF-based system). This difference can be explained by to the less bulky nature of G1 compared to THF, which creates a lower energetic hindrance upon such an interaction. Additionally, the effect of the bidentate nature of G1 is observed: the de-coordination of the initial oxygen atom requires higher energy than the subsequent one, which is seen both in the case of the first and second G1 molecules as shown in Fig. 3. Due to the small size of G1, the final structure with just one solvent molecule enables the maximization of the anion-cation interaction through up to two O_{hfip} and three F_{hfip}. Further extension of the glyme chain towards G2 slightly changes the picture (Fig. 3c). The availability of three sites for the cation coordination result in only two G2 molecules needed for full solvation. At the same time it reduces the space occupied by the solvent. The initial release of one coordination site enables the anion to approach close enough to be coordinated by two fluorine atoms. Consequently, the energy required to release the first coordination site 10 kJ mol^{-1} lower in G2 than in G1. This points out the higher ability for establishing an Mg–F contact in G2 than in G1 or THF. The subsequent release of G2 coordination sites already promotes interaction with O_{hfip}, and further removal of G2 molecules leads to the structure stabilization by two oxygen atoms of the anion. This highlights how much easier is to create aggregated structures in G2 relative to G1 and THF, confirm-

ing the chelate effect in G2: the final step of the solvent de-coordination requires the least energy. All of that underlines some important features of Mg[B($hfip$)$_4$]$_2$ salt: (i) the anion provides two types of coordination sites: higher energy sites through more available F_{hfip}, and lower energy sites through less available O_{hfip}; (ii) the effective delocalization of the negative charge inside the anion reduces the acidity of O_{hfip} to a level comparable to ethereal oxygens; (iii) the initial aggregation is hindered by the exclusive access to the F_{hfip} sites. However, if the salt concentration increases to the point where O_{hfip} becomes accessible, a massive aggregation in the system is expected. That may explain the low solubility limits of this salt in ethers, with the limit around 0.5–0.6 M for all three considered solvents. Furthermore, below that limit, aggregation can happen only through accessible F_{hfip}, which is not seen as thermodynamically preferred. Thus, a low degree of aggregation should be expected, with just a small contribution of contacted ion pairs due to the dynamic equilibrium.

We verified these hypotheses by analysing the changes in IR spectra caused by the interactions between the cation and the anion. The spectroscopic data of the electrolytes at different salt concentrations indicate only slight changes in the peak features around 1170 cm^{-1} and 860 cm^{-1}, which corresponds mainly to vibrations of CF_3 group of the anion (Fig. 4, Figure S5). To match the observed shifts with the structure, we investigate the theoretical vibrational spectra generated for all structures (Figure S6). In general, two aggregation stages can be distinguished by looking at the spectra: A minor one, where the only contact
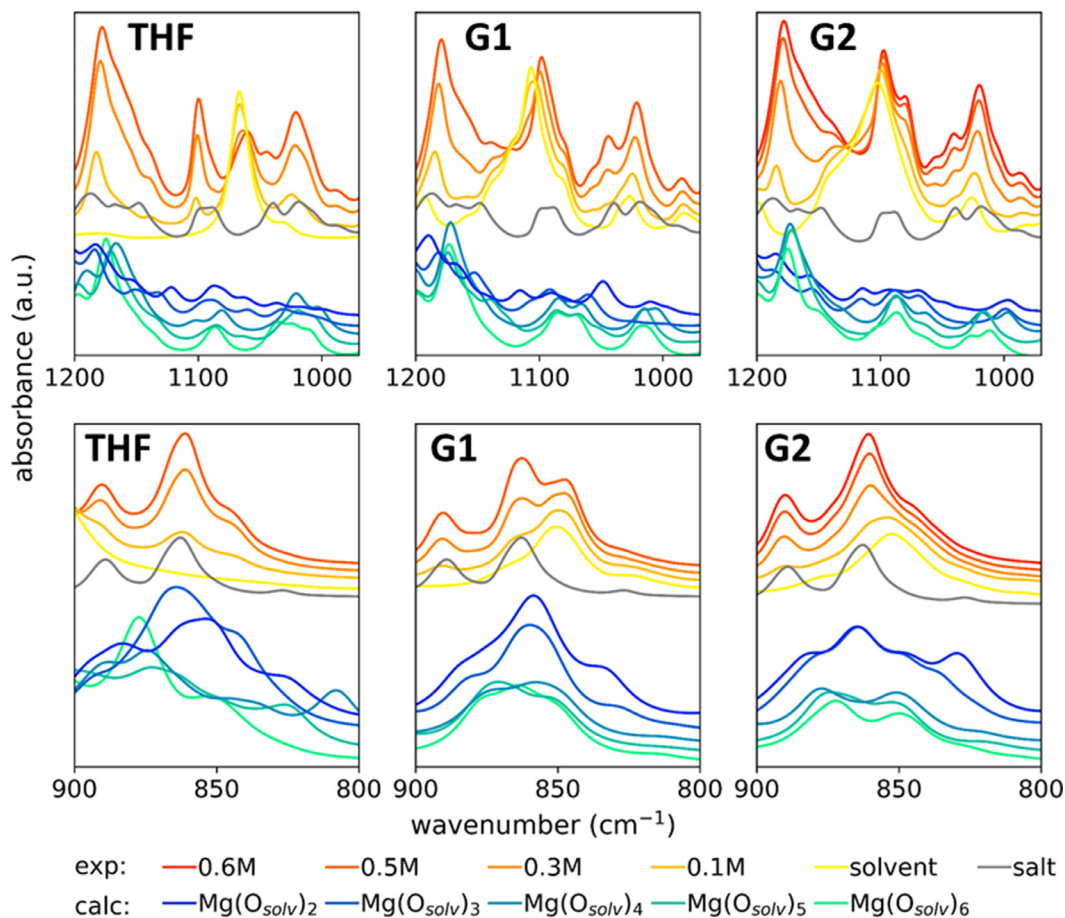
Fig. 4. Comparison of experimental and computational IR spectra for different electrolytes.

between anions and cations is through fluorine atoms F_{hfip}; and a major one where the magnesium cation get closer to the center of the anion and interacts with oxygen atoms O_{hfip}, which changes the anion geometry significantly. The initial, minor aggregation was found to cause slight shifts of the position of peaks related to CF_3 groups (redshift of ν_{CF3} at 1170cm^{-1} and $\nu_{C-C(F3)}$ at 860 cm^{-1}), B-O vibrations ν_{BO} (redshift of both asymmetric and symmetric modes at 1020 and 940 cm^{-1}, respectively), and a redshift of the solvent backbone stretching around 1100 cm^{-1}, related to decreased interaction between the solvent and the cation. Much more apparent changes were predicted for the major aggregation: a blueshift of ν_{CF3}, $\nu_{C-C(F3)}$ and δ_{CF3} around 1170, 860 and 650 cm^{-1}, respectively; along with redshift of asymmetric ν_{C-C-C} and blueshift of symmetric ν_{C-C-C} vibrations at 1380 and 1280 cm^{-1}. Looking now at the experimentally obtained spectra, no significant changes in positions of the main peaks were detected even for the electrolytes close to the solubility limit. Only small redshifts of the peaks related to ν_{CF3}, $\nu_{solvent\ backbone}$, and ν_{BO} vibrations in the range 1000–1200 cm^{-1} are visible, matching the predictions for the minor aggregation.

Additionally, some changes are observed around 860 cm^{-1}, but they are difficult to analyze due to the overlap of the ν_{C-CF3} peak of the anion with the ν_{CO} peak of solvent. However, no changes in the position of the peaks related to ν_{C-C-C} nor δ_{CF3}, at 1380–1280 cm^{-1} and 650 cm^{-1}, respectively, are observed (Figure S5) - clearly indicating that system is not able to reach any major aggregation level. Taken together, the results show that due to the unique structure of the B(hfip)$_4$$^-$ anion, the access to oxygen atoms is sterically blocked, and only the interaction through fluorine atoms is happening. Nonetheless, the energies show that such interaction is weaker than between the cation and the solvent; thus, it should be expected in a much lower degree than if other salts were used. Finally, it is important to note that such thermodynamic preference towards ions separation has beneficial consequences, especially with regard to the possible instability of the Mg^{2+}–B(hfip)$_4$$^-$ ion pair through defluorination. Still, even a small amount of ion pairs may have some effects on the electrochemical performance, and we look at this in the next section.

3.3. Stability of electrolyte against the reduction

The successful plating/stripping of metallic magnesium is the main goal of the development of magnesium electrolytes. The plating process consists of a combination of reduction and desolvation reactions. We have recently shown that the entire process is mostly limited by the initial desolvation (*i.e.*, when the magnesium loses the first solvation ligand), enabling the first electron transfer towards Mg(solvent)$_5$$^+$. [34] Further steps – second desolvation, reduction to Mg^o, and the final desolvation of the remaining solvent molecules – require much lower activation energy, mainly due to the lowered solvent interactions with the reduced cation. However, the success of such a deposition path depends on the prevention of any side reactions, which may consume electrons during the electrode process. The temporary formed metastable Mg$^+$ species are very reactive. The transfer of an electron to other components of the electrolyte must be suppressed to allow a second reduction and the final deposition of Mg^o. The unwanted electron transfer can be prevented either thermodynamically – by a higher energy of the unoccupied orbitals than the level of the electron in Mg$^+$ – or kinetically – by a high activation energy or spatial separation of the species. Such a spatial separation may be possible only in the case of anion protection at low salt concentrations. Still, it will not happen for solvent as solvent molecules surround the Mg. Since the contact of the solvent molecules with Mg$^+$ is inevitable, and to provide some background for borate-
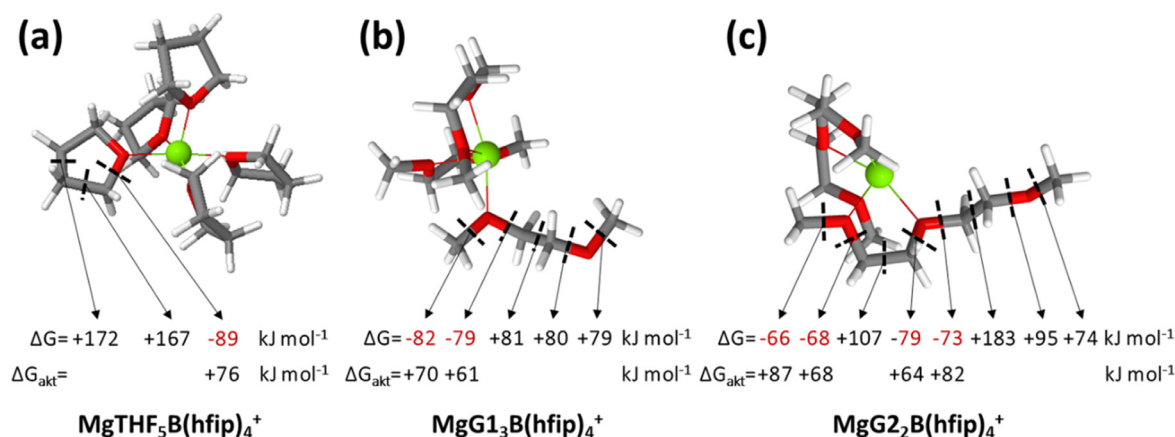
Fig. 5. The analysis of the possible solvent degradation mechanisms in a) MgTHF$_5$B(hfip)$_4^+$, a) MgG1$_3$B(hfip)$_4^+$ and c) MgG2$_2$B(hfip)$_4^+$. Values indicate predicted changes in free energy (ΔG), with negative values denoting spontaneous processes (marked in red). The activation energies (ΔG$_{akt}$) of the bond breaking are also displayed for the spontaneous processes.

Table 1
The reduction potential of one electron reduction towards Mg$^+$ of different clusters.

	E_{red}/V $vs.$ Mg		E_{red}/V $vs.$ Mg		E_{red}/V $vs.$ Mg
$6xO_{THF}$	−0.89	$6xO_{G1}$	−1.31	$6xO_{G2}$	−0.53
$5xO_{THF}+F$	−0.74	$5xO_{G1}+F$	−0.10	$5xO_{G2}+2xF$	0.19
$4xO_{THF}+2xF$	0.19	$4xO_{G1}+2xF$	0.38	$4xO_{G2}+O + 2xF$	0.30
$3xO_{THF}+O + 2xF$	0.40	$3xO_{G1}+O + 2xF$	0.45	$3xO_{G2}+2xO+2xF$	0.47
$2xO_{THF}+2xO+F$	0.56	$2xO_{G1}+2xO+2xF$	0.59	$2xO_{G2}+2xO+2xF$	0.61

based electrolytes, we first looked at the stability of the three considered solvents. We analyzed three different points on the deposition path: (i) just after transfer of the first electron – Mg(O$_{sol}$)$_5^+$, (ii) after the second desolvation - Mg(O$_{sol}$)$_4^+$ and (iii) after the second transfer of electron – Mg(O$_{sol}$)$_4^°$; where O$_{sol}$ denotes a solvent oxygen atom coordinated to the cation. As shown below, we identified the former, Mg(O$_{sol}$)$_5^+$, as the weakest step in the entire process and thus focused our analysis on that step. The analysis of the stability of two other steps on the plating path is shown in ESI for comparison (Figure S7).

In order to assess the thermodynamics of the electron transfer, we consider the cleavage of different bonds in the optimized cluster structures as a result of the solvent reduction by Mg$^+$ (Fig. 5). The results for all three solvent systems show that the most sensitive bonds are located next to the oxygen atom(s) involved in magnesium coordination. Only for these bonds, negative changes in free energy were observed, indicating a spontaneous decomposition process. The highest energetic effect is predicted for THF, −89 kJ mol^{-1}, but only a bit smaller for G1 and G2, −82 and −79 kJ mol^{-1}, respectively. Although these results indicate that the decomposition of the solvent after the electron transfer is thermodynamically favourable, it does not guarantee that the process happens. The decomposition will only occur if the process is kinetically possible. Thus, we studied the reaction paths, looking for transition states, and determining the activation energies of the process. The values are shown in Fig. 5, and pointing out the existence of large energetic barriers that slow down the decomposition process but not completely preclude it. The lowest barrier, 61 kJ mol^{-1}, was found for G1, where the release of CH$_3$O$^-$ and C$_2$H$_4$OCH$_3^•$ is the most expected. Only a slightly higher stability was observed for G2, with the weakest bond having activation energy equal to 64 kJ mol^{-1} and leading to CH$_3$OC$_2$H$_4^•$ and OC$_2$H$_4$OCH$_3^-$. The highest stability is found for THF, with an energy barrier to break the ring structure of 76 kJ mol^{-1}. The comparison of these results with those obtained for the subsequent structures on the plating path – further desolvated Mg(O$_{sol}$)$_4^+$ and reduced Mg(O$_{sol}$)$_4^°$ – clearly confirms the decreasing probability of the solvent decomposition with the progress on the reduction path (Figure S7). Both show higher activation barriers, even if the energetic effect for the latter is

much higher. Thus, Mg(O$_{sol}$)$_5^+$ stability is the determining step for the decomposition, and its degradation has to be considered during the borate electrolyte development. Such a decomposition may lead to the formation of "harder" anions, $e.g.$, CH$_3$O$^-$, which strongly interact with magnesium cations, increasing the plating overpotential. The analysis of the entire decomposition paths, together with the track of the extra electron location, is shown in Figure S8.

Having in mind the metastability of the solvent, we looked at B(hfip)$_4^-$ anion. The screening results identified unstable bonds in the anion structure upon the electron transfer from Mg$^+$: C–F bond is prone to accept an electron from Mg$^+$ and dissociate towards F^- and the remaining radical borate anion. The effect of considering the solvent explicitly coordinating the magnesium cation significantly changes the situation, as it limits contact between the cation and the anion. However, as shown in Fig. 4, magnesium was found to start forming a direct interaction with the anion through the fluorine or oxygen atoms at lower solvent content. We looked at how the structure of the electrolyte affects the reduction potential and the anion degradation. A facile electron transfer for aggregated systems was found (Table 1): fully solvated systems show negative E_{red}, requiring partial desolvation prior to reduction, confirming our previous studies [34]; the presence of the anion instead of solvent molecules makes the electron transfer easier, and the values are reaching 0 V $vs.$ Mg already after the coordination by two fluorine atoms of B(hfip)$_4^-$ anion, in case of THF- and G1-based systems. Interestingly, the reduction potentials turns positive at an earlier point for the G2-based system, as already after the first desolvation cation can coordinate two fluorine atoms, thereby increasing the reduction ability up to 0.19 V $vs.$ Mg. In general, the presence of anions in the coordination shell of magnesium has been reported many times as beneficial for electron transfer, and chlorine anions are usually employed for that. [10,35,36] The simple, mono-atomic structure of Cl$^-$ precludes any decomposition, in contrast with B(hfip)$_4^-$. The coordination of Mg$^+$ through fluorine atom(s) brings a high probability of electron transfer to the C–F bond, which we found to be the weakest in the borate anion. The energetic effect of such a transfer is quite high, more than −100 kJ mol^{-1} for all geometries (Table 2), thus higher than in the case of the

Table 2
Energetic effect of the breaking of C-F bond.

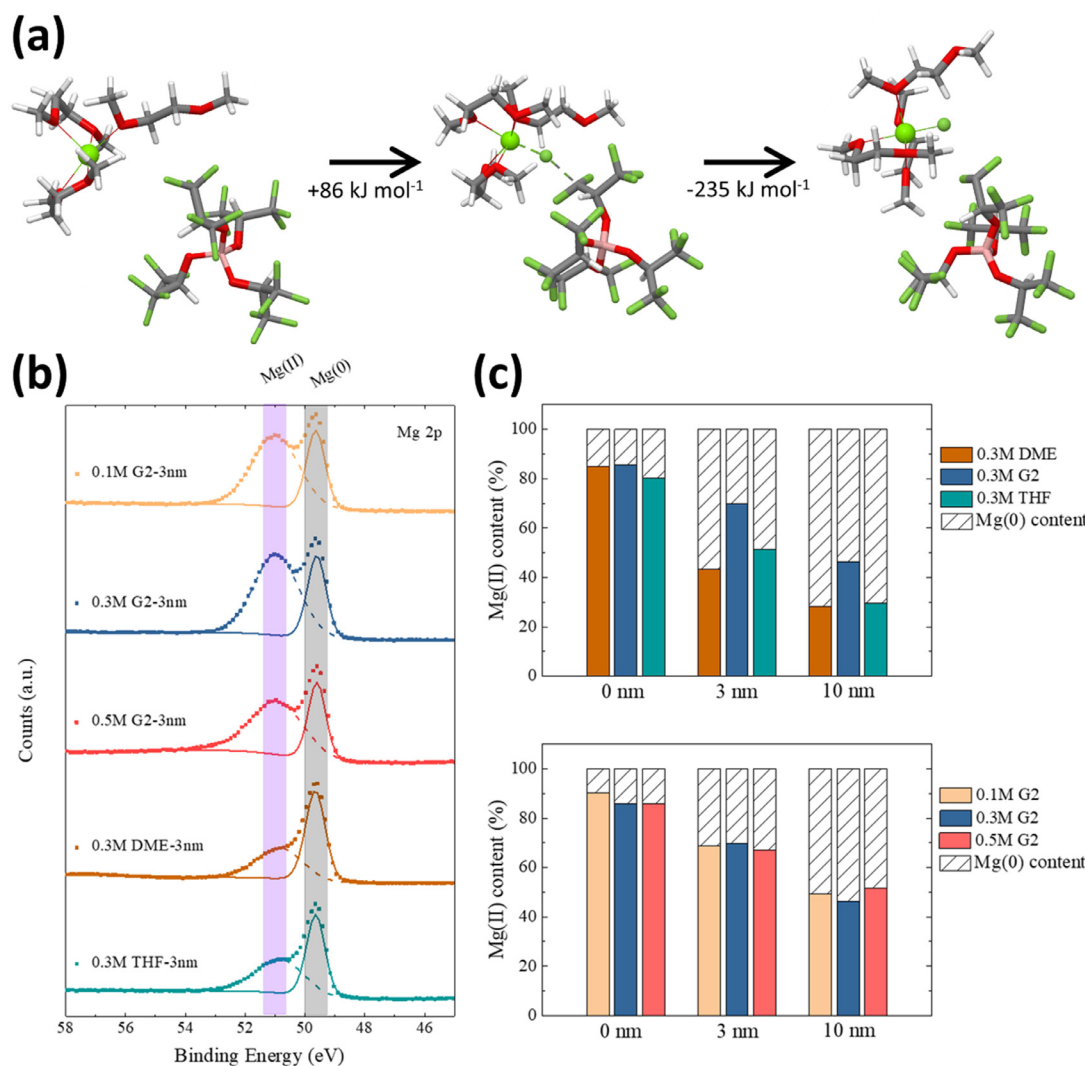|	$\Delta G/kJ\ mol^{-1}$		$\Delta G/kJ\ mol^{-1}$		$\Delta G/kJ\ mol^{-1}$
$6xO_{THF}$	−127.8	$6xO_{G1}$	−122.5	$6xO_{G2}$	−131.5
$5xO_{THF}+F$	−163.0	$5xO_{G1}+F$	−148.7	$5xO_{G2}+2xF$	−217.6
$4xO_{THF}+2xF$	−155.8	$4xO_{G1}+2xF$	−134.0	$4xO_{G2}+O+2xF$	−199.3
$3xO_{THF}+O+2xF$	−150.4	$3xO_{G1}+O+2xF$	−105.5	$3xO_{G2}+2xO+2xF$	−166.3
$2xO_{THF}+2xO+F$	−146.1	$2xO_{G1}+2xO+2xF$	−101.0	$2xO_{G2}+2xO+2xF$	−152.7

Fig. 6. (a) Geometries for anion decomposition; (b) Mg2p spectra of Mg electrodes cycled with different $Mg[B(hfip)_4]_2$-based electrolytes; (c) percentages of metallic and oxidized Mg as derived from the Mg2p spectra.

transfer to the solvent. The competition between magnesium plating, solvent, and anion decomposition is crucial and depends on the energetic barriers for all three processes. Based on the $MgG1_3B(hfip)_4$ structure, we determined the kinetic barrier for breaking the C-F bond to be a bit higher, 84 kJ mol^{-1}, as compared to solvent decomposition barriers, 61–76 kJ mol^{-1}, indicating a slightly lower probability of the decomposition of the anion under such conditions (Fig. 6a). Nonetheless, slow defluorination of anions should be expected, especially in case of G2, where the generation of unstable ion pairs is much easier.

Indeed, our XPS analysis indicates the formation of interphase at the surface of the magnesium electrode after cycling. Fig. 6b shows Mg2p spectra at 3 nm depth of the cycled electrodes with various $Mg[B(hfip)_4]_2$-based electrolytes. Two main components can be detected in all the spectra: the peak at 49.6 eV corresponds to metallic

Mg (denoted as Mg(0)), originating from Mg plating; another peak at 51.0 eV can be associated with Mg^{2+} (denoted as Mg(II)) of MgO or MgF_2, etc., which suggests the decomposition of the electrolyte. The presence of MgO and MgF_2 is supported by the corresponding O 1 s and F 1 s spectra in Figures S9-S14, with the respective peaks at ∼530.0 and ∼686.0 eV. Although bulk MgO and MgF_2 were reported to induce either a high or a moderate, respectively, Mg^{2+} migration energy barriers, the interphase does not block further Mg plating/stripping, probably due to the morphology (porous structure) and thickness (below ∼10 nm in some areas of the electrode). [32,37] Rather, it protects the bulk Mg and prevents from further electrolyte decomposition, leading to a long cycle life. A similar chemically inert interphase was also reported for reversible Mg [38] and Ca [39] plating. Fig. 6c displays the contribution of Mg(0) and Mg(II) species to the interphase at selected depths. While

similar Mg composition was found at the topmost surface, the Mg(II) species in-depth (3 nm and 10 nm) show higher content for the 0.3 M G2 electrolyte than for the 0.3 M G1 and 0.3 M THF. The result reveals some significant impact of solvent on the Mg deposition. The a bit more intense electrolyte decomposition for G2-based electrolytes is probably related to the easier connection between the anion and the cation, as shown by DFT calculations. Interestingly, varying the concentration of this electrolyte does not seem to change the composition of the deposits.

4. Conclusions

Magnesium tetrakis(hexafluoroisopropyloxy)borate has been studied many times, becoming one of the most promising salts for magnesium batteries. Our thorough evaluation of this salt aimed at explaining the impact of its structure on its electrochemical performance. We have shown that the structure of the hfip ligand represents the most optimal structural design: two highly withdrawing CF_3 groups provide high oxidation stability and low interaction energy, while the remaining proton lowers the substitution level, protecting against a reductive decomposition of the anion. The eight CF_3 groups provide a bulky nature to the anion, blocking access to the oxygen atoms hidden in its inner part. Our computational simulations indicate possible access to these inner oxygen atoms only at high salt concentrations, which due to its low solubility limit, are not reachable. The only experimentally confirmed interaction between the cation and the anion was through fluorine atoms, which is not thermodynamically favoured, keeping the salt mainly in a dissociated state. We assume that ion pairs represent only a small fraction of the salt, is the result of established equilibrium. This is very beneficial for the system's stability because contact ion pairs have been found unstable at low potentials. Their decomposition goes through the defluorination of the anion and the formation of MgF_2. The presence of MgF_2 in small amounts at the anode interface has been confirmed, which still allows the battery operation. The hindrance of anion decomposition is thanks to the rare formation of ion pairs and a bit higher energetic barrier for the electron transfer to the anion than to the solvent, making the latter more sensitive. All of that explains why $Mg[B(hfip)_4]_2$ displays a high efficiency as a salt in the electrolytes of magnesium batteries, without the need for introduction of chlorine anions to the system.

CRediT

Piotr Jankowski: Conceptualization, methodology, investigation and writing of original draft

Zhenyou Li: Methodology, investigation and writing of original draft

Zhirong Zhao-Karger: Resources and review of original draft

Thomas Diemant: Methodology, investigation and writing of original draft

Maximilian Fichtner: Resources and review of original draft

Tejs Vegge: Resources and review of original draft

Juan Maria Garcia Lastra: Conceptualization and review of original draft

Data availabilit

Data will be made available on request.

Declaration of competing Interest

The authors declare that they have no known competing financial interests or personal relationships that could have appeared to influence the work reported in this paper.

Acknowledgements

Supplementary materials

Supplementary material associated with this article can be found, in the online version, at doi:10.1016/j.ensm.2021.11.012.

References

[1] J.W. Choi, D. Aurbach, Promise and Reality of Post-Lithium-Ion Batteries with High Energy Densities, Nat. Rev. Mater. 1 (4) (2016) 1–16, doi:10.1038/natrevmats.2016.13.

[2] A. Ponrouch, J. Bitenc, R. Dominko, N. Lindahl, P. Johansson, M.R. Palacin, Multivalent Rechargeable Batteries, Energy Storage Materials 20 (2019) 253–262, doi:10.1016/j.ensm.2019.04.012.

[3] R. Dominko, J. Bitenc, R. Berthelot, M. Gauthier, G. Pagot, V. Di Noto, Magnesium Batteries: current Picture and Missing Pieces of the Puzzle, J. Power Sources 478 (2020) 229027, doi:10.1016/j.jpowsour.2020.229027.

[4] F. Liu, T. Wang, X. Liu, L.-Z. Fan, Challenges and Recent Progress on Key Materials for Rechargeable Magnesium Batteries, Adv. Energy Mater. 11 (2) (2021) 2000787, doi:10.1002/aenm.202000787.

[5] R. Dugas, J.D. Forero-Saboya, A. Ponrouch, Methods and Protocols for Reliable Electrochemical Testing in Post-Li Batteries (Na, K, Mg, and Ca), Chem. Mater. 31 (21) (2019) 8613–8628, doi:10.1021/acs.chemmater.9b02776.

[6] R. Deivanayagam, B.J. Ingram, R. Shahbazian-Yassar, Progress in Development of Electrolytes for Magnesium Batteries, Energy Storage Materials 21 (2019) 136–153, doi:10.1016/j.ensm.2019.05.028.

[7] R. Attias, M. Salama, B. Hirsch, Y. Goffer, D. Aurbach, Anode-Electrolyte Interfaces in Secondary Magnesium Batteries, Joule 3 (1) (2019) 27–52, doi:10.1016/j.joule.2018.10.028.

[8] J. Shi, J. Zhang, J. Guo, J.Interfaces in Lu, Rechargeable Magnesium Batteries, Nanoscale Horizons 5 (11) (2020) 1467–1475, doi:10.1039/D0NH00379D.

[9] J. Bitenc, K. Pirnat, E. Žagar, A. Randon-Vitanova, R. Dominko, Effect of Salts on the Electrochemical Performance of Mg Metal–organic Battery, J. Power Sources 430 (2019) 90–94, doi:10.1016/j.jpowsour.2019.04.114.

[10] P. Jankowski, J.M.G. Lastra, T. Vegge, Structure of Magnesium Chloride Complexes in Ethereal Systems: computational Comparison of THF and Glymes as Solvents for Magnesium Battery Electrolytes, Batteries & Supercaps 3 (12) (2020) 1350–1359, doi:10.1002/batt.202000168.

[11] H. Shuai, J. Xu, K. Huang, Progress in Retrospect of Electrolytes for Secondary Magnesium Batteries, Coord. Chem. Rev. 422 (2020) 213478, doi:10.1016/j.ccr.2020.213478.

[12] O. Mizrahi, N. Amir, E. Pollak, O. Chusid, V. Marks, H. Gottlieb, L. Larush, E. Zinigrad, D. Aurbach, Electrolyte Solutions with a Wide Electrochemical Window for Rechargeable Magnesium Batteries, J. Electrochem. Soc. 155 (2) (2007) A103, doi:10.1149/1.2806175.

[13] R. Schwarz, M. Pejic, P. Fischer, M. Marinaro, L. Jörissen, M. Wachtler, Magnesocene-Based Electrolytes: a New Class of Electrolytes for Magnesium Batteries, Angew. Chem. Int. Ed. 55 (48) (2016) 14958–14962, doi:10.1002/anie.201606448.

[14] M. Zoidl, C. God, P. Handel, R. Fischer, C. Lenardt, M. Schmuck, T.M. Wrodnigg, Communication—Imidazole Based Magnesium Salt as Conductive Salt for Rechargeable Magnesium-Ion Batteries, J. Electrochem. Soc. 163 (10) (2016) A2461, doi:10.1149/2.0101613jes.

[15] P. Jankowski, R. Schwarz, A. Randon-Vitanova, R. Younesi, M. Wachtler, P. Johansson, Prospects for Improved Magnesocene-Based Magnesium Battery Electrolytes, Batteries & Supercaps n/a (n/a) (2021), doi:10.1002/batt.202100040.

[16] R. Mohtadi, M. Matsui, T.S. Arthur, S.-J. Hwang, Magnesium Borohydride: from Hydrogen Storage to Magnesium Battery, Angew. Chem. 124 (39) (2012) 9918–9921, doi:10.1002/ange.201204913.

[17] O. Tutusaus, R. Mohtadi, T.S. Arthur, F. Mizuno, E.G. Nelson, Y.V. Sevryugina, An Efficient Halogen-Free Electrolyte for Use in Rechargeable Magnesium Batteries, Angew. Chem. Int. Ed. 54 (27) (2015) 7900–7904, doi:10.1002/anie.201412202.

[18] P. Jankowski, W. Wieczorek, P. Johansson, New Boron Based Salts for Lithium-Ion Batteries Using Conjugated Ligands, Phys. Chem. Chem. Phys. 18 (24) (2016) 16274–16280, doi:10.1039/C6CP02409B.

[19] Z. Zhao-Karger, M.E.G. Bardaji, O. Fuhr, M. Fichtner, A New Class of Non-Corrosive, Highly Efficient Electrolytes for Rechargeable Magnesium Batteries, J. Mater. Chem. A 5 (22) (2017) 10815–10820, doi:10.1039/C7TA02237A.

[20] I. Colomer, A.E.R. Chamberlain, M.B. Haughey, T.J. Donohoe, Hexafluoroisopropanol as a Highly Versatile Solvent, Nature Reviews Chemistry 1 (11) (2017) 1–12, doi:10.1038/s41570-017-0088.

[21] Z. Zhao-Karger, R. Liu, W. Dai, Z. Li, T. Diemant, B.P. Vinayan, C. Bonatto Minella, X. Yu, A. Manthiram, R.J. Behm, M. Ruben, M. Fichtner, Toward Highly Reversible Magnesium–Sulfur Batteries with Efficient and Practical Mg[B(Hfip)4]2 Electrolyte, ACS Energy Lett 3 (8) (2018) 2005–2013, doi:10.1021/acsenergylett.8b01061.

[22] M.J. Frisch, G.W. Trucks, H.B. Schlegel, G.E. Scuseria, M.A. Robb, J.R. Cheeseman, G. Scalmani, V. Barone, B. Mennucci, G.A. Petersson, H. Nakatsuji, M. Caricato, X. Li, H.P. Hratchian, A.F. Izmaylov, J. Bloino, G. Zheng, J.L. Sonnenberg, M. Hada, M. Ehara, K. Toyota, R. Fukuda, J. Hasegawa, M. Ishida, T. Nakajima, Y. Honda, O. Kitao, H. Nakai, T. Vreven, J.A. Montgomery Jr., J.E. Peralta, F. Ogliaro, M.J. Bearpark, J. Heyd, E.N. Brothers, K.N. Kudin, V.N. Staroverov, R. Kobayashi, J. Normand, K. Raghavachari, A.P. Rendell, J.C. Burant, S.S. Iyengar, J. Tomasi, M. Cossi, N. Rega, N.J. Millam, M. Klene, J.E. Knox, J.B. Cross, V. Bakken, C. Adamo, J. Jaramillo, R. Gomperts, R.E. Stratmann, O. Yazyev, A.J. Austin, R. Cammi, C. Pomelli, J.W. Ochterski, R.L. Martin, K. Morokuma, V.G. Zakrzewski, G.A. Voth, P. Salvador, J.J. Dannenberg, S. Dapprich, A.D. Daniels, Ö. Farkas, J.B. Foresman, J.V. Ortiz, J. Cioslowski, D.J. Fox, Gaussian 16, Revision B.01, Gaussian, Inc., Wallingford, CT, USA, 2016.

[23] Y. Zhao, D.G. Truhlar, The M06 Suite of Density Functionals for Main Group Thermochemistry, Thermochemical Kinetics, Noncovalent Interactions, Excited States, and Transition Elements: two New Functionals and Systematic Testing of Four M06-Class Functionals and 12 Other Functionals, Theor Chem Account 120 (1–3) (2008) 215–241, doi:10.1007/s00214-007-0310-x.

[24] A.-.R. Allouche, Gabedit—A Graphical User Interface for Computational Chemistry Softwares, J. Comput. Chem. 32 (1) (2011) 174–182, doi:10.1002/jcc.21600.

[25] K.-.C. Lau, T.J. Seguin, E.V. Carino, N.T. Hahn, J.G. Connell, B.J. Ingram, K.A. Persson, K.R. Zavadil, C. Liao, Widening Electrochemical Window of Mg Salt by Weakly Coordinating Perfluoroalkoxyaluminate Anion for Mg Battery Electrolyte, J. Electrochem. Soc. 166 (8) (2019) A1510, doi:10.1149/2.0751908jes.

[26] N.N. Rajput, X. Qu, N. Sa, A.K. Burrell, K.A. Persson, The Coupling between Stability and Ion Pair Formation in Magnesium Electrolytes from First-Principles Quantum Mechanics and Classical Molecular Dynamics, J. Am. Chem. Soc. 137 (9) (2015) 3411–3420, doi:10.1021/jacs.5b01004.

[27] X. Chen, H.-.R. Li, X. Shen, Q. Zhang, The Origin of the Reduced Reductive Stability of Ion–Solvent Complexes on Alkali and Alkaline Earth Metal Anodes, Angew. Chem. Int. Ed. 57 (51) (2018) 16643–16647, doi:10.1002/anie.201809203.

[28] X. Chen, X. Shen, B. Li, H.-.J. Peng, X.-.B. Cheng, B.-.Q. Li, X.-.Q. Zhang, J.-.Q. Huang, Q. Zhang, Ion–Solvent Complexes Promote Gas Evolution from Electrolytes on a Sodium Metal Anode, Angew. Chem. Int. Ed. 57 (3) (2018) 734–737, doi:10.1002/anie.201711552.

[29] X. Chen, Q. Zhang, Atomic Insights into the Fundamental Interactions in Lithium Battery Electrolytes, Acc. Chem. Res. 53 (9) (2020) 1992–2002, doi:10.1021/acs.accounts.0c00412.

[30] S. Trasatti, The Absolute Electrode Potential: an Explanatory Note (Recommendations 1986), Pure Appl. Chem. 58 (7) (2009) 955–966, doi:10.1351/pac198658070955.

[31] Y. Bouteiller, J.-.C. Gillet, G. Grégoire, J.P. Schermann, Transferable Specific Scaling Factors for Interpretation of Infrared Spectra of Biomolecules from Density Functional Theory, J. Phys. Chem. A 112 (46) (2008) 11656–11660, doi:10.1021/jp805854q.

[32] J. Forero-Saboya, C. Davoisne, R. Dedryvère, I. Yousef, P. Canepa, A. Ponrouch, Understanding the Nature of the Passivation Layer Enabling Reversible Calcium Plating, Energy Environ. Sci. 13 (10) (2020) 3423–3431, doi:10.1039/D0EE02347G.

[33] J. Drews, T. Danner, P. Jankowski, T. Vegge, J.M.G. Lastra, R. Liu, Z. Zhao-Karger, M. Fichtner, A. Latz, Modeling of Ion Agglomeration in Magnesium Electrolytes and Its Impacts on Battery Performance, ChemSusChem 13 (14) (2020) 3599–3604, doi:10.1002/cssc.202001034.

[34] J. Drews, P. Jankowski, J. Häcker, Z. Li, T. Danner, J.M. García Lastra, T. Vegge, N. Wagner, K.A. Friedrich, Z. Zhao-Karger, M. Fichtner, A. Latz, Modeling of Electron-Transfer Kinetics in Magnesium Electrolytes: influence of the Solvent on the Battery Performance, ChemSusChem n/a (n/a) (2021), doi:10.1002/cssc.202101498.

[35] N. Sa, B. Pan, A. Saha-Shah, A.A. Hubaud, J.T. Vaughey, L.A. Baker, C. Liao, A.K. Burrell, Role of Chloride for a Simple, Non-Grignard Mg Electrolyte in Ether-Based Solvents, ACS Appl. Mater. Interfaces 8 (25) (2016) 16002–16008, doi:10.1021/acsami.6b03193.

[36] A. Kopač Lautar, J. Bitenc, R. Dominko, J.-.S. Filhol, Building Ab Initio Interface Pourbaix Diagrams to Investigate Electrolyte Stability in the Electrochemical Double Layer: application to Magnesium Batteries, ACS Appl. Mater. Interfaces 13 (7) (2021) 8263–8273, doi:10.1021/acsami.0c19579.

[37] Z. Li, T. Diemant, Z. Meng, Y. Xiu, A. Reupert, L. Wang, M. Fichtner, Z. Zhao-Karger, Establishing a Stable Anode–Electrolyte Interface in Mg Batteries by Electrolyte Additive, ACS Appl. Mater. Interfaces 13 (28) (2021) 33123–33132, doi:10.1021/acsami.1c08476.

[38] B. Li, R. Masse, C. Liu, Y. Hu, W. Li, G. Zhang, G. Cao, Kinetic Surface Control for Improved Magnesium-Electrolyte Interfaces for Magnesium Ion Batteries, Energy Storage Materials 22 (2019) 96–104, doi:10.1016/j.ensm.2019.06.035.

[39] Z. Li, O. Fuhr, M. Fichtner, Z. Zhao-Karger, Towards Stable and Efficient Electrolytes for Room-Temperature Rechargeable Calcium Batteries, Energy Environ. Sci. 12 (12) (2019) 3496–3501, doi:10.1039/C9EE01699F.